

## Discrete-Time Backstepping Sliding Mode Control for a 2-DOF PAM-Based Exoskeleton

Van-Vuong Dinh<sup>1,2</sup>, Van-Long Nguyen<sup>1</sup>, Kim-Chien Hoang<sup>1</sup>,  
Minh-Duc Duong<sup>1</sup>, Quy-Thinh Dao<sup>1\*</sup>

<sup>1</sup>Hanoi University of Science and Technology, Ha Noi, Vietnam.

<sup>2</sup>Hanoi College of High Technology, Ha Noi, Vietnam.

\*Corresponding author email: [thinh.daoquy@hust.edu.vn](mailto:thinh.daoquy@hust.edu.vn)

### Abstract

This study aims to propose a discrete-time backstepping sliding mode control technique (BSMC) for regulating a pneumatic artificial muscle (PAM)-based exoskeleton used in rehabilitating human lower extremities. The PAM system is challenging to control due to its high nonlinearity, parameter uncertainty, and significant delay resulting from using compressed air. A backstepping control method is a recursive approach that systematically designs control laws for nonlinear and complicated systems. This technique ensures stable and robust system control, even in uncertain circumstances. Furthermore, the backstepping controller can handle high-order systems and guarantee high-precision tracking of a desired trajectory. The incorporation of sliding mode control is aimed at enhancing the performance of the robot PAM system by reducing chattering and reaching time. The algorithm employs Lyapunov functions and sliding surfaces to design the control signal for operating the system. The study concludes with experimental scenarios demonstrating the effectiveness of the proposed approach.

Keywords: Pneumatic artificial muscle, backstepping, sliding mode control

### 1. Introduction

Rehabilitation robots are often expensive due to their high manufacturing cost, mainly because electric motors power them [1, 2]. However, a growing interest is in developing low-cost robots that can operate efficiently. In recent years, pneumatic artificial muscles (PAMs) have emerged as one of the most promising actuators for simulating human movements. PAMs are lightweight, low-cost, and easy to manufacture. The power-to-weight ratio is also a significant concern. Therefore, researchers are increasingly studying PAMs and their applications in rehabilitation robots, medical devices for motor function recovery, and control programs to enhance human safety while working with robots. The cylindrical braided muscle [3], known as McKibben's in the 1950s, is currently the most popular type of artificial pneumatic muscle. Besides the mentioned advantage [4] PAMs have several limitations, including high nonlinearity, uncertain parameters, and high impact delay. Therefore, modeling and control pneumatic artificial muscles have recently become an interesting topic for researchers.

Regarding the design of control algorithms for rehabilitation robots using pneumatic artificial muscles, we have two main control algorithms: Linear and nonlinear control. For linear control, since most of

the objects in practice are nonlinear, we often linearize these objects to simplify the control. However, the system will only work well within certain limits. The PAMs system mentioned in this paper is nonlinear, with considerable latency and uncertain parameters. Such systems always attract great attention from researchers. The problem with these systems of PAMs is determining a nonlinear mathematical model that leads to errors in estimating the system's parameters. As a result, PAM-based systems have a lot of unknown disturbances. Multiple control methods have been offered to solve the problems of pneumatic muscle actuator control. The Proportional-Integral-Derivative (PID) controller and its enhanced versions are the most researched. For example, a nonlinear PID-based controller [5, 6] enhances the correction of nonlinear hysteresis phenomena and increases robustness. The Fuzzy PID controllers [7, 8] are offered to increase the trajectory tracking performance. The neural network PID controllers [9, 10] are trained to provide the optimum value for various set frequencies and load conditions. Most of the mentioned controllers have decent performance and specific advantages and disadvantages. However, the PID controller is also unsuitable for objects with high nonlinearity and delay characteristics, so it does not guarantee the optimization and stability of the system.

This paper proposes the BSMC algorithm as one of the most widely used approaches for highly nonlinear systems. BSMC is a distinct nonlinear control technique integrating the backstepping control design approach and sliding mode control controller. The Backstepping control law, developed in the 1990s by Petar V. Kokotovic and other researchers [11], is designed to develop stabilizing controls for a particular category of nonlinear dynamical systems. It is a nonlinear control approach with the primary advantage of handling complex nonlinear systems and disturbances, making it applicable to various applications.

Moreover, backstepping can be utilized to design robust controllers insensitive to modeling errors and uncertainties while providing better tracking and disturbance rejection performance compared to other control techniques. These nonlinear dynamical systems are composed of subsystems that extend from a primary subsystem, which can be stabilized using another method. The recursive structure of the system enables the designer to commence the design process at the stable subsystem and sequentially stabilize each outer subsystem by developing new controllers using a "backing out" approach. In this study, we aim to stabilize the control variables, such as acceleration, velocity, and the joint angle corresponding to the robot. The algorithm will rely on the selection of Lyapunov functions and sliding surfaces to design the control signal that will stabilize the system according to Lyapunov [12, 13]. By incorporating backstepping and sliding mode control, the proposed algorithm provides more effectiveness than the conventional sliding control algorithm [14-16]. To summarize, this paper makes the following contributions:

- Development of a discrete-time backstepping sliding mode control for a pneumatic artificial muscle-based exoskeleton;
- The proposed controller's effectiveness is demonstrated through various experimental scenarios to verify its suitability for robotic rehabilitation systems utilizing a pneumatic artificial muscle actuator.

The paper's structure is as follows: Section 2 outlines the experimental platform, equipment, and a mathematical model of a PAM-based exoskeleton. Section 3 describes the design of the proposed controller. Section 4 demonstrates the experimental results. Lastly, section 5 summarizes the research and discusses possible future work.

## 2. Robotic System Modeling

Fig. 1 illustrates a robot system that utilizes a pneumatic artificial muscle actuator. This system is designed for lower extremity rehabilitation and features a hip and knee joint affixed to a flat surface to facilitate movement. A pair of pneumatic artificial

muscles, installed in an antagonistic configuration with one another through a pulley, drive each joint. Specifically, a 1-inch-diameter McKibben artificial muscle was utilized, which, like human muscles, has a maximum contraction of 30% of muscle length. The proportional control valve ITV2030-212S-X26 from sliding mode control (SMC) is employed for PAMs' pressure adjustment. The rotation angles are measured using a WDD35D4 rotary potentiometer coaxially mounted to two couplings.

In addition, loadcell sensors are installed on the single-ended muscle tubes to measure the pulling force of each muscle. The control algorithm is implemented using the NI Myrio platform, developed by National Instrument. The NI Myrio control computer acquires voltage signals from various sources, including loadcells and potentiometers. The control program is then developed and compiled using Labview software and downloaded to NI Myrio to create a closed-loop control system.

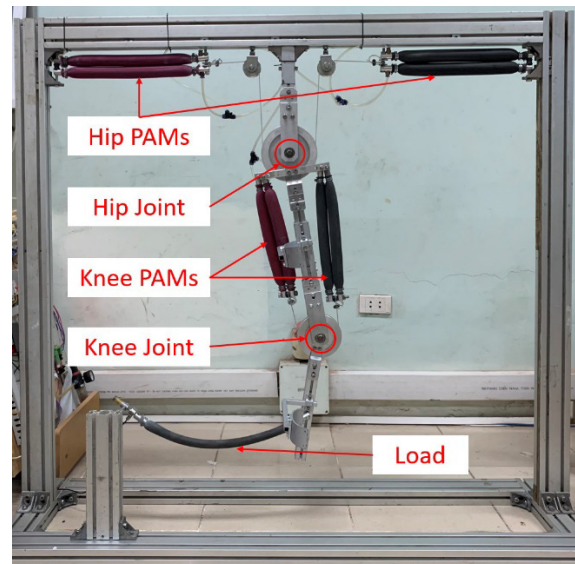


Fig. 1. The experimental model of a robot system using a pneumatic artificial muscle actuator.

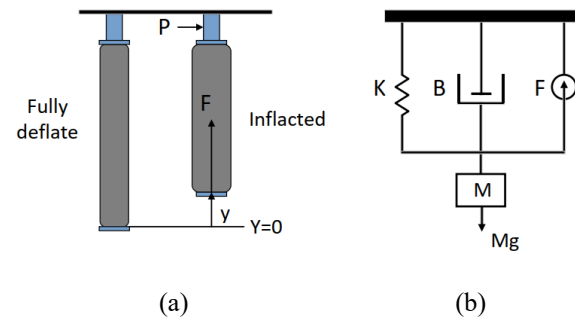


Fig. 2. (a) The schematic diagram of PAM. (b) The three-element model of PAM.

To model the PAM robot system, we refer to Reynolds's three-element model [17] of a single PAM as shown in Fig. 2. Accordingly, the model can be represented by the equation:

$$M \ddot{y} + B(P)\dot{y} + K(P)y = F(P) - Mg \quad (1)$$

with

$$\begin{cases} K(P) = K_0 + K_1P \\ B(P) = B_{0i} + B_{1i}P \quad (\text{inflation}) \\ B(P) = B_{0j} + B_{1j}P \quad (\text{deflation}) \\ F(P) = F_0 + F_1P \end{cases}$$

where  $y$  is the amount of the PAM contraction.  $K(P)$ ,  $B(P)$ ,  $F(P)$  are the model's spring, damping, and contractile elements.  $P$  is the input pressure of the PAM. The parameter value  $B$  will depend on when the PAM contracts  $B_i$  or deflates  $B_j$ .

The robotic system is designed to operate as follows: Each joint of the robotic orthosis is actuated by two PAMs in an antagonistic setup. In this setup, each joint's anterior and posterior muscles have been initially provided with similar pressure  $P_0$ . Therefore they have the same length. We create rotation by increasing the pressure on one side of the muscle while the pressure on the other decreases  $\Delta P$ . Therefore,  $\Delta P$  is the control variable. A detailed description of the structure of the robot system is shown in Fig. 3.

Let the input pressure of the anterior muscles ( $P_a$ ) and posterior muscles ( $P_p$ ) are:

$$\begin{cases} P_a = P_0 + \Delta P + P_{AP} \\ P_p = P_0 - \Delta P \end{cases} \quad (2)$$

The initial different pressure  $P_{AP}$  is added so the robot is upright at the initial position.

The contraction of the anterior muscle ( $y_a$ ) and posterior muscle ( $y_p$ ) can be determined using the following equations:

$$\begin{cases} y_a = y_0 - R\theta \\ y_p = y_0 + R\theta \end{cases} \quad (3)$$

where  $R$  is the radius of the joint,  $y_0$  is the muscle's initial contraction, and  $\theta$  is the joint's rotation angle.

Based on the report [18], the torque generated can be expressed as follows:

$$T = \left[ (F_a - K_a y_a - B_a \dot{y}_a) - (F_p - K_p y_p - B_p \dot{y}_p) \right] R \quad (4)$$

where  $F_a$ ,  $K_a$ , and  $B_a$  depend on the input pressure of anterior muscle and  $F_p$ ,  $K_p$ , and  $B_p$  depend on the input pressure of posterior muscle according to (1).

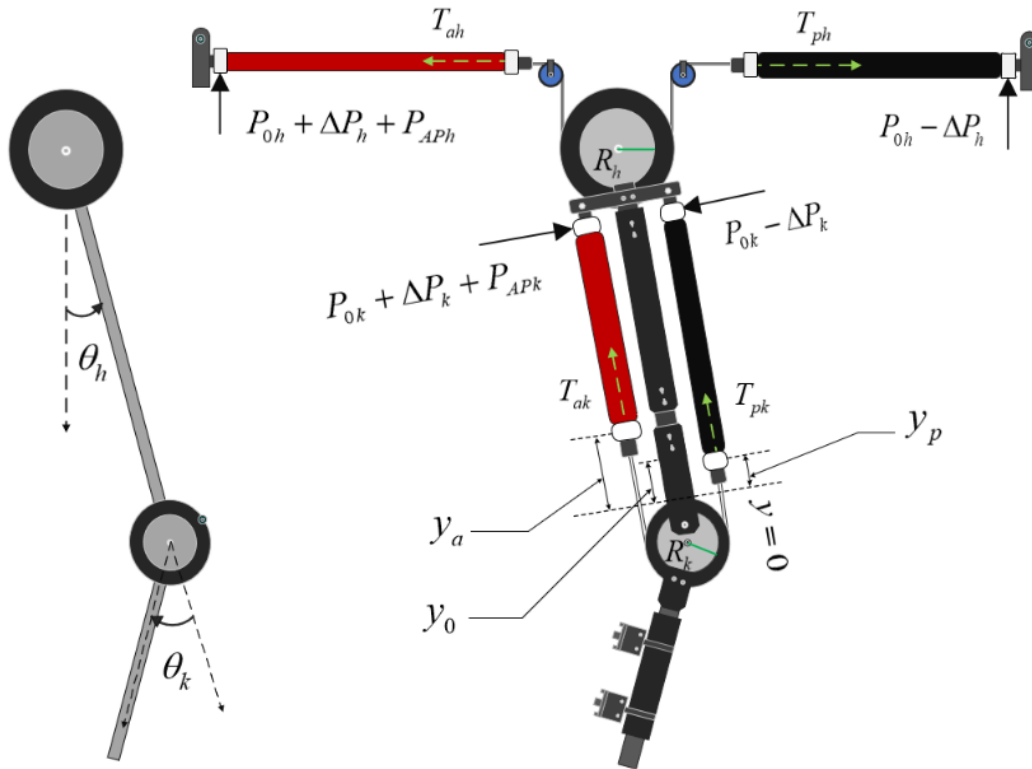


Fig. 3. The structure of hip and knee muscles with an antagonistic configuration

Thus,

$$\begin{aligned} T = & \left[ F_1 P_{AP} + 2K_0 R \theta - K_1 (P_{AP} y_a + P_0 y_a - P_0 y_p) \right. \\ & \left. - (B_{0a} + B_{1a} P_0 + B_{1a} P_{AP}) \dot{y}_a + (B_{0p} + B_{1p} P_0) \dot{y}_p \right] R \\ & + [2F_1 - B_{1a} \dot{y}_a + B_{1p} \dot{y}_p] R \Delta P \end{aligned} \quad (5)$$

Substituting  $y_a$ ,  $y_p$  from to (3) into (5). The torque T created by anterior and posterior PAMs to the joint can be obtained as follows:

$$T = c_1 + c_2 \theta + c_3 \dot{\theta} + c_4 \Delta P \quad (6)$$

where

$$\begin{cases} c_1 = F_1 P_{AP} R \\ c_2 = (2K_0 + 2K_1 P_0 + K_1 P_{AP}) R^2 \\ c_3 = [B_{0a} + B_{0p} + (B_{0a} + B_{0p}) P_0 + B_{1a} P_{AP}] R^2 \\ c_4 = 2F_1 R - (B_{1a} - B_{1p}) R^2 \dot{\theta} \end{cases}$$

From the torque of the PAM-based actuator in equation (6), we consider the dynamic behavior of the PAM-based 2-DOF robot as the following equation:

$$\mathbf{H}\ddot{\boldsymbol{\theta}} + \mathbf{V}\dot{\boldsymbol{\theta}} + \mathbf{J} = \mathbf{T} \quad (7)$$

Here,  $\boldsymbol{\theta} = \begin{bmatrix} \theta_h \\ \theta_k \end{bmatrix}$  represents the coordinates of the

robot joints and  $\mathbf{T} = \begin{bmatrix} T_h \\ T_k \end{bmatrix}$  represents the torque matrix

generated by the effects of the PAMs on the robot's joints. Additionally  $\mathbf{H}$ ,  $\mathbf{V}$ ,  $\mathbf{J}$  denote the inertia, viscous moment and radial force matrices, and the gravity torque matrix.

From (6) and (7), we have:

$$\mathbf{H}\ddot{\boldsymbol{\theta}} + \mathbf{V}\dot{\boldsymbol{\theta}} + \mathbf{J} = \mathbf{c}_1 + \mathbf{c}_2 \boldsymbol{\theta} + \mathbf{c}_3 \dot{\boldsymbol{\theta}} + \mathbf{c}_4 \Delta P \quad (8)$$

Thus

$$\ddot{\boldsymbol{\theta}} = \mathbf{H}^{-1} (-\mathbf{V}\dot{\boldsymbol{\theta}} - \mathbf{J}') + (\mathbf{H}^{-1} \mathbf{c}_4) \Delta P \quad (9)$$

with  $\begin{cases} \mathbf{V}' = \mathbf{V} - \mathbf{c}_3 \\ \mathbf{J}' = \mathbf{J} - \mathbf{c}_2 \boldsymbol{\theta} - \mathbf{c}_1 \end{cases}$

where  $\mathbf{c}_1 = \begin{bmatrix} c_{1h} \\ c_{1k} \end{bmatrix}$ ,  $\mathbf{c}_2 = \begin{bmatrix} c_{2h} & 0 \\ 0 & c_{2k} \end{bmatrix}$ ,  $\mathbf{c}_3 = \begin{bmatrix} c_{3h} & 0 \\ 0 & c_{3k} \end{bmatrix}$

$\mathbf{c}_4 = \begin{bmatrix} c_{4h} & 0 \\ 0 & c_{4k} \end{bmatrix}$ ,  $\Delta P = \begin{bmatrix} \Delta P_h \\ \Delta P_k \end{bmatrix}$ ,  $h$ , and  $k$  denote the hip and knee joints, respectively. By including the term  $\boldsymbol{\psi}(t)$ , which denotes the unknown disturbance that

exists in the system, the state-space model of the dynamic system (9) can be represented as follows:

$$\begin{cases} \dot{\mathbf{x}}_1(t) = \boldsymbol{\theta}(t) \\ \dot{\mathbf{x}}_2(t) = \dot{\boldsymbol{\theta}}(t) \\ \dot{\mathbf{x}}_3(t) = \mathbf{f}(\mathbf{x}_1(t), \mathbf{x}_2(t), \boldsymbol{\psi}(t)) \\ \quad + (\Delta \boldsymbol{\lambda} \boldsymbol{\psi}(t) + \boldsymbol{\lambda}) \mathbf{u}(t) \end{cases} \quad (10)$$

where  $\begin{cases} \mathbf{f}(t) = \mathbf{H}^{-1} (-\mathbf{V}'\dot{\boldsymbol{\theta}} - \mathbf{J}') \\ \boldsymbol{\lambda} = \mathbf{H}^{-1} \mathbf{c}_4 \\ \mathbf{u}(t) = \Delta P \end{cases}$

Assume  $\mathbf{y}(k)$ ,  $\mathbf{y}_1(k)$ ,  $\mathbf{y}_2(k)$  are the muscle's matrix, velocity, and acceleration, respectively. The discrete-time model for the dynamic system of PAM can be obtained from the following:

$$\begin{cases} \mathbf{y}(k+1) = \mathbf{y}(k) + T_s \mathbf{y}_1(k) \\ \mathbf{y}_1(k+1) = \mathbf{y}_1(k) + T_s \mathbf{y}_2(k) \\ \mathbf{y}_2(k) = \mathbf{f}(\mathbf{y}_1(k), \mathbf{y}_2(k), \boldsymbol{\psi}(k)) \\ \quad + (\Delta \boldsymbol{\lambda} \boldsymbol{\psi}(k) + \boldsymbol{\lambda}) \mathbf{u}(k) \end{cases} \quad (11)$$

By setting  $\boldsymbol{\zeta}(k) = \mathbf{f}(\mathbf{y}_1(k), \mathbf{y}_2(k), \boldsymbol{\psi}(k)) + \Delta \boldsymbol{\lambda} \boldsymbol{\psi}(k) \mathbf{u}(k)$ , the model (11) becomes:

$$\begin{cases} \mathbf{y}(k+1) = \mathbf{y}(k) + T_s \mathbf{y}_1(k) \\ \mathbf{y}_1(k+1) = \mathbf{y}_1(k) + T_s \mathbf{y}_2(k) \\ \mathbf{y}_2(k) = \boldsymbol{\zeta}(k) + \boldsymbol{\lambda} \mathbf{u}(k) \end{cases} \quad (12)$$

### 3. Controller Design

This section introduces the proposed BSMC technique, which has two primary goals: Maintaining system stability and regulating the mechanical rotation angle  $y(k)$  to track a reference signal  $y^*(k)$ , that mimics the actual motion of the human foot. Fig. 4 depicts the control block diagram of the BSMC approach. The backstepping control method decomposes the second-order system model into smaller subsystems. At each stage, the virtual control law  $y_1(k)$  and  $y_2(k)$  for the corresponding subsystems are developed using the discrete-time Lyapunov stability theorem. With strictly Lyapunov stability functions, the recursive algorithm assures the proposed BSMC strategy's internal dynamic stability. In step 3, the sliding-mode control approach guarantees that the system state trajectory reaches the sliding surface and that the system disturbance current tracking error reduces to zero.

STEP 1: Aims to establish a tracking error vector that measures the difference between the controlled rotation angle  $y(k)$  and the reference signal  $y^*(k)$ :

$$e(k) = y(k) - y^*(k) \quad (13)$$

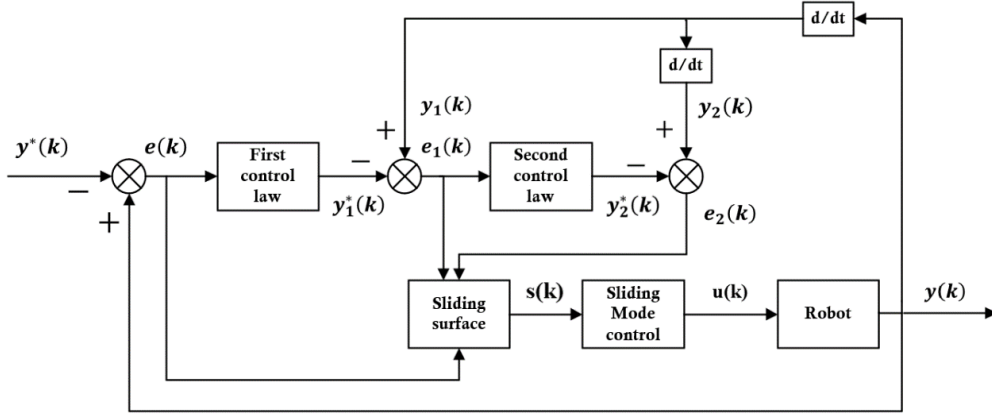


Fig. 4. Block diagram of the controller.

Select the initial Lyapunov function candidate as:

$$V_1(k) = e(k)^2 \quad (14)$$

Hence, the variation of  $V_1(k)$  can be obtained as:

$$\begin{aligned} \Delta V_1(k) &= V_1(k+1) - V_1(k) \\ &= [y(k+1) - y^*(k+1)]^2 - e(k)^2 \\ &= [y(k) + T_s e_1(k) + T_s y_1^*(k) \\ &\quad - y^*(k+1)]^2 - e(k)^2 \end{aligned} \quad (15)$$

The initial virtual control law vector is denoted as  $y_1(k)$  can be expressed as the first vector in the sequence of virtual control laws, starting with  $y_1^*(k)$  in step 1, which is defined as follows:

$$y_1^*(k) = \frac{y^*(k+1) - y(k)}{T_s} \quad (16)$$

Substituting (16) into (15) yields:

$$\begin{aligned} \Delta V_1(k) &= [T_s y_1(k) - T_s y_1^*(k)]^2 - e(k)^2 \\ &= T_s^2 e_1(k)^2 - e(k)^2 \end{aligned} \quad (17)$$

STEP 2: To guarantee the convergence of the vector  $e_1(k)$  to zero, we can choose the second Lyapunov function as:

$$V_2(k) = e_1^2(k) + V_1(k) \quad (18)$$

Using (13), it is possible to derive the error vector for  $e_2$  as:

$$\begin{aligned} e_1(k+1) &= y_1(k+1) - y_1^*(k+1) \\ &= y_1(k) + T_s y_2(k) - y_1^*(k+1) \end{aligned} \quad (19)$$

The derivative of  $V_2(k)$  can be calculated as:

$$\begin{aligned} \Delta V_2(k) &= e_1(k+1)^2 - e_1(k)^2 + \Delta V_1(k) \\ &= (y_1(k) + T_s y_2(k) - y_1^*(k+1))^2 \\ &\quad - (1 - T_s^2) e_1(k)^2 - e(k)^2 \end{aligned} \quad (20)$$

We can define the first virtual control law vector  $y_2^*(k)$  in step 1 as follows, with  $y_2(k)$  representing the initial virtual control law vector:

$$y_2^*(k) = \frac{y_1^*(k+1) - y_1(k)}{T_s} \quad (21)$$

Substituting (21) into (20), we have:

$$\begin{aligned} \Delta V_2(k) &= [T_s y_2(k) - T_s y_2^*(k)]^2 \\ &\quad - (1 - T_s^2) e_1(k)^2 - e(k)^2 \\ &= [T_s e_2(k)]^2 - (1 - T_s^2) e_1(k)^2 - e(k)^2 \end{aligned} \quad (22)$$

By examining (22), it becomes evident that  $\Delta V_2(k)$  will become negative definite if  $e_2(k)$  equals 0. Therefore, the next stage is determining the vector of  $e_2(k)$  that leads to convergence towards zero.

STEP 3: At this stage, a sliding-mode control approach is applied after completing the two steps in the backstepping design process. The sliding-surface vector is formulated as:

$$s(k) = e_2(k) + \alpha e_1(k) + \beta e(k) \quad (23)$$

where  $\alpha$  and  $\beta$  are positive constants, a third candidate for the Lyapunov function is defined as:

$$V_3(k) = s(k-1)^2 + V_2(k) \quad (24)$$

The derivative of  $V_3(k)$  can be obtained as:

$$\begin{aligned} \Delta V_3(k) &= s(k)^2 - s(k-1)^2 + \Delta V_2(k) \\ &= s(k)[e_2(k) + \alpha e_1(k) + \beta e(k)] \\ &\quad - s(k-1)^2 + [T_s e_2(k)]^2 \\ &\quad - (1 - T_s^2) e_1(k)^2 - e(k)^2 \end{aligned} \quad (25)$$

The calculated deviation  $e_2(k)$  is:

$$\begin{aligned} e_2(k) &= y_2(k) - y_2^*(k) \\ &= -y_2^*(k) - \zeta(k) - \lambda u(k) \end{aligned} \quad (26)$$

In the proposed BSMC method, it is assumed that the control law vector has the following structure:

$$\begin{aligned} u(k) &= \lambda^{-1} \left[ -y_2^*(k) - \zeta(k) - \rho \text{sign}(s(k)) \right. \\ &\quad \left. - (2 + \gamma)e_2(k) - \alpha e_1(k) - \beta e(k) \right] \end{aligned} \quad (27)$$

where  $\gamma$  is a positive number added to satisfy the condition  $\Delta V_3(k) \leq 0$  in equation (29).

Subsequently, the derivative of  $V_3(k)$  can be represented as:

$$\begin{aligned} \Delta V_3(k) &= s(k) \left[ -\gamma e_2(k) \right] - \rho s(k) \text{sign}(s(k)) \\ &\quad - s(k-1)^2 + [T_s e_2(k)]^2 \\ &\quad - (1 - T_s^2) e_1(k)^2 - e(k)^2 \end{aligned} \quad (28)$$

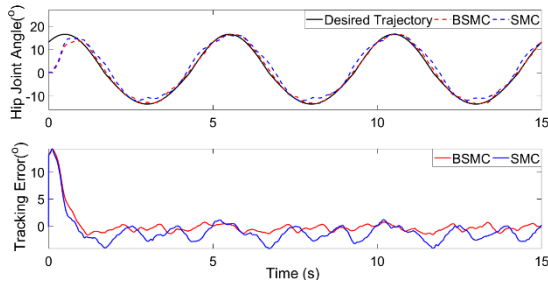
We can arrive at the following equation by replacing (28) with (27):

$$\begin{aligned} \Delta V_3(k) &\leq -s(k-1)^2 - \left[ e(k) + \frac{\gamma\beta}{2} e_2(k) \right]^2 \\ &\quad - (1 - T_s^2) \left[ e_1(k) + \alpha\gamma \frac{e_2(k)}{2(1 - T_s^2)} \right]^2 \\ &\quad - \left[ \gamma - \frac{\gamma^2\beta^2}{4} - \frac{\alpha^2\gamma^2}{4(1 - T_s^2)} - T_s^2 \right] e_2(k)^2 \end{aligned} \quad (29)$$

Equation (29) enables the selection of a set of numbers  $\alpha, \beta$  and  $\gamma$  that ensure the stability of the Lyapunov function. Therefore, the proposed backstepping sliding mode control guarantees the system's stability.

#### 4. Experimental Results

We will compare the control performance achieved by implementing the BSMC and SMC



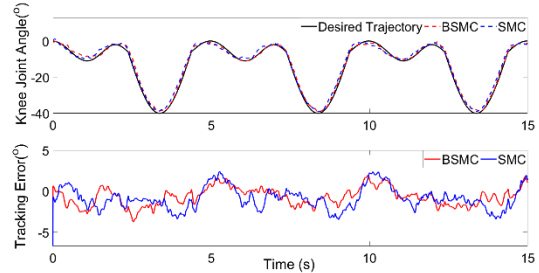
(a) Hip joint

algorithms on the rehabilitation robot to evaluate the efficacy of the control methodology presented. The hip and knee angle reference trajectories will be adjusted for each subject by modifying the gait data profile in [19], with the hip and knee flexion/extension angles ranging from  $-13.5^\circ$  to  $16.5^\circ$  and  $-40^\circ$  to  $0^\circ$ , respectively. The control algorithm will be developed using the Lab-VIEW/MyRIO toolkit and then integrated into the MyRIO 1900 controller with a 5 ms sampling time. We will test multiple scenarios to evaluate and improve the practicality of the control method. Specifically, the experiment will be conducted at frequencies of 0.2 Hz or 0.5 Hz under two scenarios: with and without a load. The parameters for both the BSMC and SMC controllers will be fine-tuned and summarized in Table 1.

Table 1. Parameters of the BSMC and SMC controllers

Parameters	$\rho$	$\alpha$	$\beta$	$\gamma$
BSMC	0.025	0.1	1	0.5
SMC	0.025	0.1		

Both control strategies demonstrate effective tracking performance in the first scenario without a load. The joint angle signals of the robot tracked the sample trajectory and achieved a steady state in less than  $\frac{1}{4}$  cycle gait. However, the BSMC controller outperforms the SMC controller with higher performance and fewer errors, as demonstrated in Fig. 5 and Fig. 6. Specifically, the SMC controller exhibits an oscillation amplitude of about  $3.8^\circ$  for the hip joint, while the BSMC controller's amplitude is only about  $1.4^\circ$  and the deviation value fluctuates around  $0^\circ$ . At 0.5 Hz, both control methods exhibit reduced performance, but the BSMC controller is still better at tracking the trajectory. The effectiveness of the proposed controller is further demonstrated by the root mean square error (RMSE) values, which are  $3.46^\circ$  and  $2.11^\circ$  for the hip and knee joints, respectively, with the BSMC controller. In comparison, the SMC controller produces RMSE values of  $3.89^\circ$  and  $2.68^\circ$  for the same joints.



(b) Knee joint

Fig. 5. Experimental results when tracking joint trajectory at 0.2 Hz without a load.

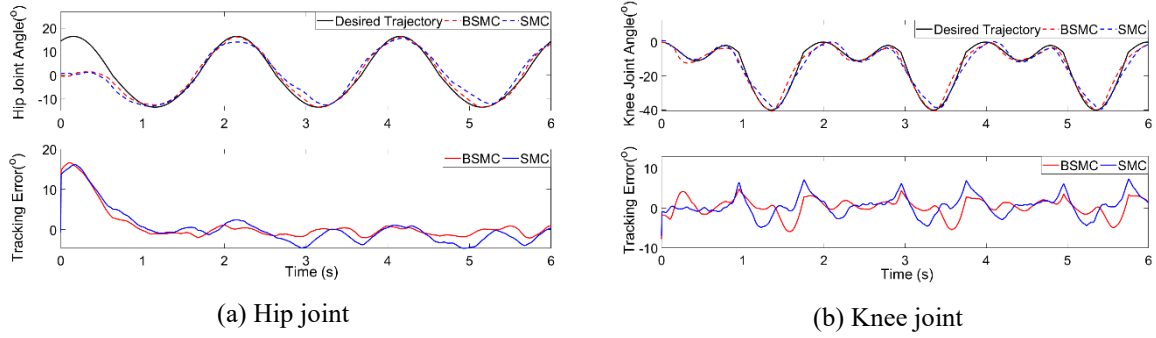


Fig. 6. Experimental results when tracking joint trajectory at 0.5 Hz without a load.

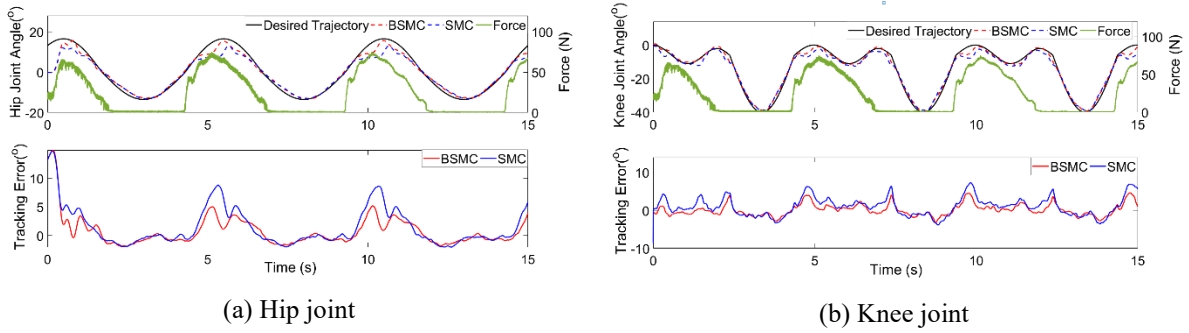


Fig. 7. Experimental results when tracking joint trajectory at 0.2 Hz with a load.

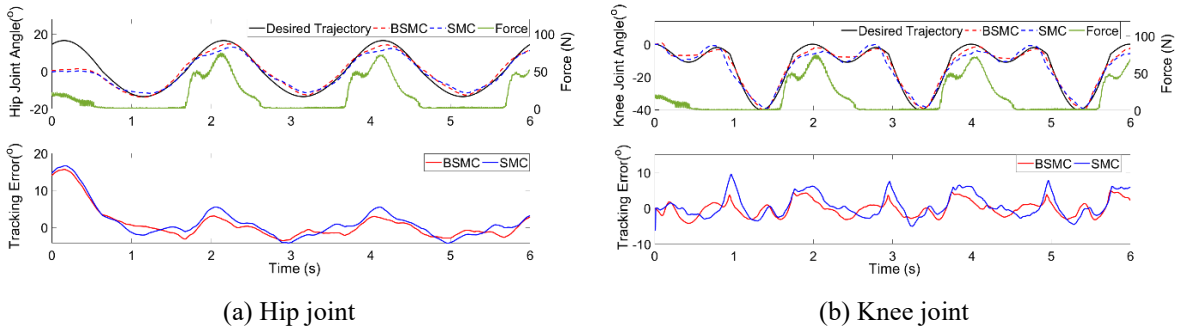


Fig. 8. Experimental results when tracking joint trajectory at 0.5 Hz with a load.

In the second scenario, where the rehabilitation robot is subjected to external loads, the performance of both controllers is decreased but still achieves satisfactory accuracy. This scenario is significant because rehabilitation robots typically encounter external forces and loads in practical applications. The load is placed at the position of the lower limb exoskeleton robot, and the maximum impact force is experienced when the leg is extended forward. We use anthropometric data (described in Table 4 in the book [20]) to determine the Rated Load to be applied quantitatively. Since the study only focused on lower extremity rehabilitation, the experiment will be implemented with a variable load weighing 60 kg to 80 kg. The ratio of total leg weight to total body weight is 0.161. Each robot only controls one human leg, from which we calculate the rated Load ranging from 48.3 N to 64.44 N. The author changed the Load as the Load variable with the value from 0 N to 75.44 N.

Specifically, the explanation was also highlighted on page 7 of the revised manuscript. As illustrated in Fig. 7, when observing the hip and knee angles with a frequency of 0.2 Hz, the BSMC controller demonstrates faster stabilization times. As the applied force gradually increases to the maximum value, the tracking error of BSMC stabilizes quickly, while SMC spikes up quite high. When monitored at 0.2 Hz, SMC's highest deviation of dynamic performance is around 9.0°, whereas BSMC's figure is approximately 5.0°. At a frequency of 0.5 Hz, the BSMC controller demonstrates a lower root mean square error (RMSE) of 4.30° and 2.65° for the hip and knee joints, respectively. In contrast, the SMC controller produces RMSE values of 4.79° and 3.26° for the same joints. Finally, the RMSE values of BSMC in Table 2 and Table 2 demonstrate that it outperforms the SMC controller.

Table 2. RMSE (°) of two controllers with hip joint trajectory input.

Frequency	Without load		Load	
	BSMC	SMC	BSMC	SMC
0.2 Hz	2.29	2.61	2.77	3.59
0.5 Hz	3.46	3.89	4.30	4.79

Table 3. RMSE (°) of two controllers with knee joint trajectory input.

Frequency	Without load		Load	
	BSMC	SMC	BSMC	SMC
0.2 Hz	1.29	1.59	1.76	2.59
0.5 Hz	2.11	2.68	2.65	3.26

Table 4. ISE (°) of two controllers with hip joint trajectory input.

Frequency	Without load		Load	
	BSMC	SMC	BSMC	SMC
0.2 Hz	78.39	112.58	103.36	140.58
0.5 Hz	104.06	135.62	125.71	154.87

Table 5. ISE (°) of two controllers with knee joint trajectory input.

Frequency	Without load		Load	
	BSMC	SMC	BSMC	SMC
0.2 Hz	25.20	38.10	30.48	57.50
0.5 Hz	49.27	109.07	57.20	118.52

Table 6. IAE (°) of two controllers with hip joint trajectory input.

Frequency	Without load		Load	
	BSMC	SMC	BSMC	SMC
0.2 Hz	18.78	20.35	22.45	29.43
0.5 Hz	30.43	34.27	32.63	38.10

Table 7. IAE (°) of two controllers with knee joint trajectory input.

Frequency	Without load		Load	
	BSMC	SMC	BSMC	SMC
0.2 Hz	15.76	20.44	16.67	23.02
0.5 Hz	22.67	27.79	24.24	31.53

We calculated additional Integral Absolute Error (IAE), Integral Squared Error (ISE) to contrast the performance between SMC relatively and suggested

BSMC. The results in Table 4, Table 5, Table 6, and Table 7 still show that the proposed BSMC controller performs better. ISE integrates the square of the error over time. Therefore, this index will increase sharply when a large overshoot. This is most clearly demonstrated when observing the knee angles with a frequency of 0.5 Hz. While the ISE Index of the BSMC controller is 57.20°, that of the SMC controller is up to 118.52°. IAE integrates the absolute error over time. Therefore in the same case, the IAE index will be smaller than ISE's. Specifically, the knee angles with a frequency of 0.5 Hz is also observed. The ISE Index of BSMC and SMC controller is 24.24° and 31.53°, respectively.

### 5. Conclusion

This paper proposes and applies the BSMC law to the PAM-based robot to aid in the recovery of leg muscle function for patients. The proposed controller can manage the PAM robot's direction, velocity, and acceleration based on desired references. The backstepping law aims to mitigate chattering and enhance the SMC method's tracking capabilities during transient and steady-state operations. The tracking precision of the BSMC controller is evaluated, and the efficacy of the reaching law is confirmed via various experimental scenarios. The outcomes of the experiments indicate that the proposed controller successfully addresses chattering issues and delivers adequate tracking performance. The proposed BSMC controller performs similarly with and without load compared to SMC. For instance, when tracking a knee joint with 0.2 Hz and 40° amplitude without load, the BSMC controller's RMSEs reach 1.29° (3.23% of amplitude), while the SMC controller achieves an accuracy of 5.7%. In summary, the BSMC controller reduces tracking errors and enhances performance when tracking human gait patterns. The results suggest the potential of this controller in rehabilitation robots. However, the tracking error remains significant. Additional control laws may be necessary to restore patient function, such as using neural networks to recognize human impedance and tracking errors.

### Acknowledgments

This research was funded by Hanoi University of Science and Technology (HUST) under project number T2022-PC-002.

### References

- [1] M. al Kouzbary, N. A. Abu Osman, A. K. Abdul Wahab, Sensorless control system for assistive robotic ankle-foot, *Int J Adv Robot Syst*, vol. 15, no. 3, May 2018, <https://doi.org/10.1177/1729881418775854>.
- [2] Z. Wang, L. Quan, and X. Liu, Sensorless SPMSM position estimation using position estimation error suppression control and EKF in wide speed range, *Math Probl Eng*, vol. 2014, 2014, <https://doi.org/10.1155/2014/480640>.

- [3] M. G. Antonelli, P. Beomonte Zobel, A. De Marcellis, and E. Palange, Design and characterization of a McKibben pneumatic muscle prototype with an embedded capacitive length transducer, *Machines*, vol. 10, no. 12, Dec. 2022, <https://doi.org/10.3390/machines10121156>.
- [4] S. M. Mirvakili, I. W. Hunter, *Artificial muscles: mechanisms, applications, and challenges*, *Advanced Materials*, vol. 30, no. 6. Wiley-VCH Verlag, Feb. 2018, <https://doi.org/10.1002/adma.201704407>.
- [5] J. Zhong, J. Fan, Y. Zhu, J. Zhao, and W. Zhai, One nonlinear pid control to improve the control performance of a manipulator actuated by a pneumatic muscle actuator, *Advances in Mechanical Engineering*, vol. 2014, 2014, <https://doi.org/10.1155/2014/172782>.
- [6] G. Andrikopoulos, G. Nikolakopoulos and S. Manesis, Non-linear control of Pneumatic Artificial Muscles, 21st Mediterranean Conference on Control and Automation, Patanias, Greece, 2013, pp. 729-734, <https://doi.org/10.1109/MED.2013.6608804>.
- [7] J. Wu, J. Huang, Y. Wang, K. Xing and Q. Xu, Fuzzy PID control of a wearable rehabilitation robotic hand driven by pneumatic muscles, 2009 International Symposium on Micro-NanoMechatronics and Human Science, Nagoya, Japan, 2009, pp. 408-413, <https://doi.org/10.1109/MHS.2009.5352012>.
- [8] A. Koohestani and E. A. Moghadam, Controlling muscle-joint system by functional electrical stimulation using combination of PID and fuzzy controller, *APCBEE Procedia*, vol. 7, pp. 156-162, 2013, <https://doi.org/10.1016/j.apcbee.2013.08.027>.
- [9] J. Zhao, J. Zhong, and J. Fan, Position control of a pneumatic muscle actuator using RBF neural network tuned PID controller, *Math Probl Eng*, vol. 2015, 2015, <https://doi.org/10.1155/2015/810231>.
- [10] P. Pathak, S. B. Panday, and J. Ahn, Artificial neural network model effectively estimates muscle and fat mass using simple demographic and anthropometric measures, *Clinical Nutrition*, vol. 41, no. 1, pp. 144-152, Jan. 2022, <https://doi.org/10.1016/j.clnu.2021.11.027>.
- [11] P. V. Kokotovic, The joy of feedback: nonlinear and adaptive, in *IEEE Control Systems Magazine*, vol. 12, no. 3, pp. 7-17, June 1992, <http://doi.org/10.1109/37.165507>.
- [12] Y. Kim, T. H. Oh, T. Park, and J. M. Lee, Backstepping control integrated with Lyapunov-based model predictive control, *J Process Control*, vol. 73, pp. 137-146, Jan. 2019, <https://doi.org/10.1016/j.jprocont.2018.12.007>.
- [13] T. Liard, I. Ismaila Balogoun, S. Marx, and F. Plestan, Boundary sliding mode control of a system of linear hyperbolic equations: a Lyapunov approach, 2021. [Online]. Available: <https://www.sciencedirect.com/science/article/pii/S005109821004908>
- [14] J. Wang, J. Liu, G. Zhang, and S. Guo, Periodic event-triggered sliding mode control for lower limb exoskeleton based on human-robot cooperation, *ISA Trans*, vol. 123, pp. 87-97, Apr. 2022, <https://doi.org/10.1016/j.isatra.2021.05.039>.
- [15] L. Melkou and M. Hamerlain, High Order Homogeneous Sliding Mode Control for a Robot Arm with Pneumatic Artificial Muscles, *IECON 2019 - 45th Annual Conference of the IEEE Industrial Electronics Society*, Lisbon, Portugal, 2019, pp. 394-399, <https://doi.org/10.1109/IECON.2019.8927339>.
- [16] L. Zhao, H. Cheng, and T. Wang, Sliding mode control for a two-joint coupling nonlinear system based on extended state observer, *ISA Trans*, vol. 73, pp. 130-140, Feb. 2018, <https://doi.org/10.1016/j.isatra.2017.12.027>.
- [17] D. B. Reynolds, D. W. Repperger, C. A. Phillips, and G. Bandry, Modeling the dynamic characteristics of pneumatic muscle, *Ann Biomed Eng*, vol. 31, no. 3, pp. 310-317, 2003, <https://doi.org/10.1114/1.1554921>.
- [18] T. Y. Choi and J. J. Lee, Control of manipulator using pneumatic muscles for enhanced safety, *IEEE Transactions on Industrial Electronics*, vol. 57, no. 8, pp. 2815-2825, Aug. 2010, <https://doi.org/10.1109/TIE.2009.2036632>.
- [19] C. Schreiber, F. Moissenet, A multimodal dataset of human gait at different walking speeds established on injury-free adult participants, *Sci Data*, vol. 6, no. 1, Dec. 2019, <https://doi.org/10.1038/s41597-019-0124-4>.
- [20] D. A. Winter, *Biomechanics and Motor Control of Human Movement*, John Wiley & Sons, 2009. <https://doi.org/10.1002/9780470549148>